Lab on a Chip

Accepted Manuscript

ROYAL SOCIETY OF CHEMISTRY

www.rsc.org/loc

Beating heart on a chip: a novel microfluidic platform to generate functional 3D cardiac microtissues

Anna Marsano[1], Chiara Conficconi[1,2]*, Marta Lemme[1,2]*, Paola Occhetta[2], Emanuele Gaudiello[1], Emiliano Votta[2], Giulia Cerino[1], Alberto Redaelli[2], and **Marco Rasponi[2]**

[1] Departments of Surgery and Biomedicine, University Basel, University Hospital Basel, Basel, Switzerland

[2] Department of Electronics, Information and Bioengineering, Politecnico di Milano, Milano, Italy

* These authors equally contributed to this work

Corresponding authors

Marco Rasponi
Piazza Leonardo da Vinci 32
Building #21
20133 Milano, Italy.
Tel.: +39 02 2399 3377
Fax: +39 02 2399 3360
Email: marco.rasponi@polimi.it

Anna Marsano
Cardiac Surgery and Engineering Group
Department of Biomedicine, Hebelstrasse 20
4031 Basel, Switzerland
Tel.: +41 061 32 87448
Fax.: +41 061 265 3990
Email: anna.marsano@usb.ch

Abstract

In the past years microfluidic-based technology developed microscale models recapitulating key physical and biological cues typical of the native myocardium. However, the application of controlled physiological uniaxial cyclic strains on defined three-dimension cellular environment was not yet possible. Two-dimension mechanical stimulation was particularly investigated neglecting the complex three-dimensional cell-cell and cell-matrix interactions. For this purpose, we developed a heart-on-a-chip platform, which recapitulates the physiologic mechanical environment experienced by cells in the native myocardium. The device includes an array of hanging posts to confine cell-laden gels, and a pneumatic actuation system to induce homogeneous uniaxial cyclic strains to the 3D cell constructs during culture.

The device was used to generate mature and highly functional micro-engineered cardiac tissues (μECTs), from both neonatal rat and human induced pluripotent stem cell-derived cardiomyocytes (hiPSC-CM), strongly suggesting the robustness of our engineered cardiac micro-niche. Our results demonstrated that the cyclic strain was effectively highly uniaxial and uniformly transferred to cells in culture. As compared to control, stimulated μECTs showed superior cardiac differentiation, as well as electrical and mechanical coupling, owing to a remarkable increase in junction complexes. Mechanical stimulation also promoted early spontaneous synchronous beating and better contractile capability in response to electric pacing. Pacing analyses of hiPSC-CM constructs upon controlled administration of isoprenaline showed further promising applications of our platform in drug discovery, delivery and toxicology fields.

The proposed heart-on-a-chip device represents a relevant step forward in the field, providing a standard functional three-dimensional cardiac model to possibly predict signs of hypertrophic changes in cardiac phenotype by mechanical and biochemical co-stimulation.

Introduction

The organ-on-a-chip technology aims at mimicking the native cellular milieu by recapitulating fundamental organ-specific dynamic conditions in microfluidic cell culture devices[1]. Miniaturization to the micrometer scale offers several advantages as superior control over the local cellular microenvironment[2, 3] and significant reduction in the use of compounds, reagents and cells, therefore increasing the experimental throughput in a cost effective manner. Although the heart is one of the most investigated organs, the implementation of physiological biochemical and biophysical cues at the cellular environment still needs further advancement to generate reliable and functional micro-cardiac tissues[4].

The crucial biochemical and physical signals capable to instruct cells and guide them through tissue development and maturation are influenced by the local heart tissue "niche"[5-9]. In particular, cardiomyocytes (CM) are subjected *in vivo* to contraction/relaxation phases during each heartbeat. This continuous deformation is perceived by cells as a cyclic uniaxial strain along the locally oriented extracellular matrix (ECM) fibers, and is known to activate mechano-sensitive signaling pathways, in turn affecting the characteristics of cardiac cells themselves[10-12]. A robust and predictive *in vitro* model of mature cardiac tissues should thus enable the recapitulation of (i) the three-dimensional (3D) architecture of complex cell-cell and cell-ECM interactions and (ii) electro-mechanical stimuli resembling the native myocardial environment[13], (iii) in the presence of controlled biochemical signals.

Microfluidic platforms have been widely exploited for the generation of 3D micro-tissue models with well-defined architectures[14]. The working principle of these devices relies on an inner core channel, delimited by rows of rigid posts, serving as cage for the forming cell construct. A recent alternative layout of this design allowed to densely pack and culture human induced pluripotent stem cell-derived CM (iPSC-CM). Thanks to dedicated channels, this cardiac microphysiological system was used to assess the effect of drugs on cardiac cells spontaneous pacing[15]. However, the

monolithic design of this platform precluded the integration of any mechanical stimulation mechanism.

Indeed, the application of a mechanical strain has recently showed beneficial effects on self-assembly, maturation and functionality of micro-cardiac tissues whether obtained from murine progenitors or iPSC-CM[6, 16]. These results were achieved by generating cardiac micro wires (CMW) in an elegant microscale platform able to promote the self-assembling of cell-laden collagen fibers, and subsequently their maturation by imposing an auxotonic load. However CMW suffer from a few drawbacks: their final size and shape cannot be directly controlled; the mechanical stimulation is not tunable, being highly dependent on the specific CMW maturation; the auxotonic contraction is not properly representative of the adult native mechanical environment. Furthermore, although microscale tissues, CMW are not generated within a microfluidic environment; indeed, the ability to generate mature and functional micro-cardiac tissues directly within a microfluidic platform still remains crucial to guarantee the fine control, and hence the effective and reproducible testing of the dose dependent effect of drugs and chemicals[17].

It is common belief that a platform able to provide controlled cyclic strain could dramatically improve engineered cardiac tissue contractile performance and level of maturation[18, 19]. The application of uniaxial cyclic strain has been widely used to enhance functionality on 2D cell monolayers[20-22]. However, its translation to 3D models has not been yet achieved, mainly due to technical difficulties in accurately controlling the strain of micrometer-sized tissues characterized by poor mechanical properties.

Here, we report a new method to generate mature and highly functional micro-cardiac tissues within a microfluidic device. To this purpose, we developed an innovative heart-on-chip platform for the culture of 3D cell constructs, able to mimic the mechanical stimulation experienced by cells in the native myocardium. The presence of auxiliary channels beyond the culture chamber allowed perfusing medium during culture, while providing biochemical stimulation and transporting pacing signals during the functional evaluation of tissues.

In this study, we assess the effects of the application of physiological cyclic uniaxial strains (10-15%) on maturation and functionality of well-defined geometry micro-engineered cardiac tissues (μECTs), generated by neonatal rat or human iPSC-CM.

Results

Device design and fabrication

An array of hanging posts was conceived to define the culture channel (Fig. 1a). Although not completely closed, this caging structure is enough to contain a cell-laden pre-polymer solution throughout the injection and subsequent polymerization phases. Once the 3D cell construct is generated, gaps underneath posts serve to precisely define a stroke length for the actuation mechanism. Indeed, upon pressurization of an auxiliary compartment (Fig. 1b), a flexible membrane moves upwards, thus inducing a uniaxial strain to the 3D cell construct. When the pressure is released, elastic recoil causes the membrane and the 3D cell construct to relax to their original size. A cyclic pressure signal can thus mimic systolic and diastolic phases in a tunable fashion.

The micro-bioreactor was realized by assembling multiple layers of polydimethylsiloxane (PDMS). PDMS was chosen as the main material due to its favourable features in cell culture applications (namely gas permeability and optical transparency) and the robustness of soft-lithography techniques as fabrication method[23]. In addition, its elastic mechanical properties were relevant to implement embedded deformable parts able to apply controlled strains to cells.

The assembly process is schematically depicted in Fig 1c. The device comprises three layers. Two layers facing each other form the cell culture compartment, where cells and culture medium are hosted; in particular, the top layer contains two rows of posts, intended for hosting the cell construct (300μm wide), while the bottom layer is an open bath with the function of creating hanging posts with a controlled gap. Both distance between pillars and pillar gap were set equal to 50μm to allow cell-laden gel confinement during injection[24]. The injection process of a coloured gel is illustrated in the Movie S1. A third layer constitutes the actuation compartment; once pressurized, it has the function to deform the membrane between compartments. Due to the low aspect ratio of this latter layer (1.6mm wide, 50μm high), two rows of scaffolding posts were included to prevent PDMS buckling. Additional details are provided in the Online Methods.

As shown in Fig. 1d, seven access holes connect the micro-bioreactor to the external world. The cell culture compartment (green in the figure) is equipped with two connection ports for cell injection, and four reservoirs for cell culture medium replacement. The actuation compartment (red in the figure) is provided with a single port connecting the device to an electro-pneumatic controller. A picture of the actual assembled device is shown in Fig. 1e, placed in a 30mm Petri dish, while a scanning electron microscopy (SEM) micrograph of the device cross-section is reported in Fig. 1f, showing both compartments, separated by the PDMS membrane.

Mechanical characterization of the device

To assess whether the deformation imposed to cells is unidirectional when the underlying PDMS membrane is loaded, a finite element model (FEM) of the microfluidic platform was built (Fig. 2a,b, Fig. S1 and Movie S2) and the nominal strains (NE) within the gel bulk were quantified. Over the majority of the gel bulk, the applied elongation resulted roughly uniaxial. Nominal strains in the pillar-to-pillar direction (NE_{xx}) were the only positive normal strain component and ranged between 10% and 15%, while strains in the direction of the membrane movement (NE_{yy}) were about -35% (Fig. S1b), consistently with the compression due to the designed stroke length, and strains in the direction of the channel axis (NE_{zz}) were almost negligible, ranging between -2.5% and 2.5% (Fig. S1c). Relevant deviations from this pattern were limited to the region immediately adjacent to the pillar (Fig. 2 and Fig. S1).

To verify the numerical results, the microfluidic device was integrated with a pressure regulator system through an electronically controlled solenoid valve, so that an overpressure signal in the actuation compartment produced a cyclic stretching of the 3D cell construct. Repeated measurements of the global nominal strains (ε) of the real 3D gel construct were performed during the cycle of mechanical stimulation on microscopic images through ImageJ software, based on the positions of the spherical polystyrene beads immobilized in fibrin gel (Fig. 2d). Experimental ε_{xx} and ε_{zz} at maximal elevation of the deformable membrane resulted in 12.52% ± 3.90% and -0.59%

± 3.63%, respectively. These measurements were mimicked on the numerical model; the displacements of nodes of the computational grid representative of the beads' position were computed and the corresponding nominal strains were derived. Computed ε_{xx} and ε_{zz} at maximal elevation resulted in 13.60% ± 4.59% and -1.49% ± 1.72%, respectively, well matching experimental values.

The mechanical stretching also resulted in a corresponding cell shape distortion, as visualized by concomitant increases in the projected area and length of cardiac fibroblast cells embedded in fibrin gel in the direction of applied tension (Movie S3).

Cell proliferation and viability

Freshly isolated neonatal rat cardiac cells were seeded into the microfluidic platform by means of fibrin gel and subsequently cultured either under cyclic mechanical stimulation (10% uniaxial strain, 1 Hz frequency; Movie S4) or in static condition as control. The initial cell population was composed predominantly by cardiomyocytes (84.9% ± 1.9%, identified by cardiac troponin I) and fibroblasts (15.0% ± 1.9%, identified by vimentin), as quantified through image analysis of monolayer adherent cells. A similar cell composition was found in 3D cardiac micro-tissues (78.5% ± 4.3% cardiomyocytes and 20.4% ± 2.7% fibroblasts) (Fig 3a).

One day after injection, proliferating cardiac fibroblasts, positive for Ki67, were observed both at the centre and at the edges of the micro-constructs (Fig. 3b). However, the application of cyclic uniaxial strain enhanced cell proliferation already after one day in culture, as shown by a significantly higher percentage of proliferating cells (12.8% ± 1.0%) as compared to 3D static control (7.9% ± 0.7%) (Fig. 3b). After 5 days in culture the majority of cells resulted to be alive in both conditions. However, the ethidium and Calcein AM staining showed that cell viability was significantly enhanced in the stimulated micro-constructs compared to 3D static control (84.11% ± 1.3% vs 67.51% ± 0.9%, Fig. 3c).

Neonatal rat CM-based 3D micro-cardiac construct maturation

Cardiomyocytes were capable to mature in both control and stimulated conditions, as underlined by the elongated, rod-like morphology, typical of cardiomyocytes, depicted by immunofluorescence staining specific for α-sarcomeric actinin (Fig. 4a) and cardiac troponin I (Fig. 4b,c). A slightly higher concentration of cells was also evident in both the control and stimulated tissues in the proximity of micro-post rows. Cx43 -the main form of gap junctions expressed in the heart- appeared to be functionally present at the extracellular membrane of cardiomyocytes predominantly in the stimulated micro-tissues (Fig. 4c). The total $Cx43^{+}$ area normalized to the number of cardiomyocytes indeed resulted statistically higher for the stimulated constructs as compared to the static control (45.4 ± 4.8 and 29.1 ± 3.1 μm^2, respectively) (Fig. 4d). Mechanically stimulated and statically cultured constructs showed also similar expressions at the mRNA level of specific cardiac markers (e.g. MYH7, MYH6, MLC2v, MLC2a, Troponin I, Cx43 and N-cadherin) (Fig. S6). Only the mRNA expression of MYH6, indicative of less developed cardiac phenotype, decreased in mechanically stimulated micro-tissues, resulting therefore also in a superior ratio of MYH7 / MYH6, implying a superior maturation stage (Fig. 4e and Fig. S6). The overall quality of cardiac micro-tissues indeed resulted to be superior in terms of both micro- and ultra- structure when mechanical stimulation was applied (Fig. S7). While statically cultured cardiac cells appeared to be embedded in the original fibrin gel, the mechanically stimulated constructs showed a superior remodelling of the embedding vehicle substituted by newly deposited extracellular matrix (Fig. S7a). At the ultra-architecture level, cells exposed to cyclic strain showed a more complex organization of the sarcomeric structures as evidenced by the presence of intercalated discs and gap junctions (Fig. S7b). The difference in the level of cell electrical junctions between static and stimulated μECTs was also confirmed by a different behaviour of the micro-cardiac constructs in terms of spontaneous contractile activity. Although spontaneous contraction was documented already after three days in culture in both conditions, only samples cultured under cyclic mechanical stimulation showed a synchronous contractile activity throughout the micro-cardiac constructs

(Movies S5 and S6), as confirmed by the quantitative analysis of contraction peaks in multiple randomly selected regions of the cell constructs (Fig. 5a,b). Indeed, the transmission of electrical potential is facilitated by the increased presence of low resistance membrane areas (namely gap junctions).

Contractile properties of the micro-tissues in response to electrical pacing were also improved after mechanical stimulation (Fig. 5c-e). The excitation threshold (ETH) was significantly lower in the stimulated constructs as compared to controls (0.38±0.15V vs. 0.86±0.04V), whereas the maximum capture rate (MCR) resulted to be slightly higher. Furthermore, the contraction amplitude (3.1±0.4% vs. 1.3±0.8%) was significantly higher after exposing the constructs to cyclic uniaxial strain. In the Fig. 5f, representative tracings are reported to evidence the higher contraction rate of stimulated constructs.

Human iPSC-CM -based 3D micro-cardiac construct maturation

Human iPSC-CM were embedded in fibrin gel prior to injection into the microdevices immediately after thawing, and exposed to mechanical stimulation (10% uniaxial strain, 1 Hz frequency). After 6 days of culture most of the iPSC-CM expressed specific cardiac troponin I and exhibited an elongated cardiac-like morphology (Fig. 6a). Human iPSC-CM achieved a rather mature phenotype, as confirmed by the presence of functional gap and adherens junctions like Cx43 and N-Cadherin, respectively (Fig. 6b). N-cadherin -the main cardiac isoform of the adherens junctions- is also located transmembranly as Cx43. The observed increase in the expression of two main junctional complexes most likely supported both the propagation of electrical stimuli throughout heart cells and provided mechanical coupling to cardiomyocytes. The human cardiac micro-tissues began a spontaneous beating already at day 2.5±0.5 (Movie S7). The ETH resulted to be even lower as compared to the corresponding tissues derived from rat (0.18±0.16 V/cm vs. 0.86±0.04 V/cm). The MCR was similar to the control rat micro-tissues and 1.5-fold lower as compared to those stimulated (Fig. 6c).

The human cardiac micro-tissues were tested for their response to supplementation of isoprenaline, a β1- and β2-adrenoreceptor agonist, commonly used to treat bradycardia or heart block, in both presence or absence of an external electrical pacing signal (Fig. 6d). During pacing (at a frequency of 1 Hz and 1.5-fold ETH) an increase of the contraction rate was observed in micro tissues when 0.1 nM of isoprenaline was reached. Without the electrical pacing, instead, the beating frequency was accelerated at 10 nM of isoprenaline, while the contraction rate kept increasing in a dose-dependent manner up to 1000nM.

Discussion

In this study we introduced a method to generate mature and functional 3D cardiac micro-constructs and to assess their performance upon specific drug supplementation within a microfluidic environment.

In most of the *in vitro* microscale systems currently available, cardiac cells are cultured on flat membranes and exposed to 2D cyclic mechanical strains[25, 26]. However, these 2D high-throughput platforms fail to recapitulate the cell-cell and cell-extracellular matrix interactions typical of the complex 3D structural environment of the native myocardium. An attempt to generate 3D micro-heart tissues is represented by the so-called cardiac microwire (CMW) technology[16]. This method is based on a pair of flexible cantilevers, designed to constrain a neo-forming tissue: by exploiting the predominantly uniaxial intra-tissue forces, the growing micro-tissue remodels forming a linear band. However, this approach does not allow to precisely control the CMW geometry, and the cyclic deformations occurring in the native cardiac tissue are not reproduced.

Aiming at replicating the physiological strains at which a small section of the native heart are locally exposed, we developed a new microscale biomimetic platform integrating for the first time (i) the ability to generate 3D cell constructs with well-defined geometries from cell-laden hydrogel pre-polymers, (ii) an active mechanical stimulation module, and (iii) microfluidic channels for the efficient delivery of drugs and chemicals. The key-feature of this heart-on-chip device is the ability to integrate in a microfluidic platform a simple mechanism able to convert a pressure signal into a controlled uniform uniaxial cyclic strain provided to 3D cell cultures. The design was optimized with the implementation of a FEM numerical model, whose effectiveness was assessed through experimental measures.

The heart-on-chip device was employed to generate micro-engineered cardiac tissues (μECTs), with well-defined dimensions (300μm wide, 150μm high and 10mm long), from either neonatal rat or human iPSC-derived cardiomyocytes. In both conditions, cyclic mechanical stimulation showed to improve the maturation of the μECTs, evidenced by an increase of electrical and mechanical

coupling among neighbouring cells as compared to controls. In rat micro-tissues the expression at the mRNA level of typical markers of cardiac maturation (e.g. higher MHY7/MHY6 ratio) was found to be higher than in controls. Accordingly, spontaneous beating and contractility parameters upon external electric pacing resulted to be enhanced by the mechanical stimulation. These results are in good agreement with Thavandiran *et al.*[16]. However, when considering human cardiomyocytes, auxotonic stimulation yielded unstable CMW tissues, able to generate asynchronous contractions, while synchronous beating was only achieved upon enrichment of the cardiomyocyte population with fibroblasts[16]. Remarkably, µECTs generated in our platform from human iPSC-CM started sustained and synchronous beating activity already after 2.5 days in culture, and responded to electric pacing signals with an electric potential threshold 10-fold lower than the stimulated CMW. Although the multi-sheet architecture of the myocardium is not yet achieved, these results demonstrate the fundamental importance of the replication also of small section of the native mechanical environment, which is three-dimensional and cyclic in nature, provided by the proposed heart-on-chip technology. Indeed, the ability to generate reproducible and functional cardiac micro-tissues from human iPSC-CM broadens the application horizons of this device, with the possibility to generate patient-specific myocardium-like tissues modelling unique and relevant genetic cardiac disorders[27]. As a proof-of-principle, human µECTs were used as reliable cardiac surrogate responding to the supplementation of drugs in a physiological manner. Spontaneously contracting human cardiac micro-tissues indeed responded to concentrations of isoprenaline (ß-adrenergic stimulation) as low as 1nM with a positive chronotropic effect, as previously described in large- and micro-scale human embryonic cells at 100nM and 1µM, respectively[28, 29] and iPSC-CM in monolayer at 0.08µM[30].

Although µECTs were here generated by using a commercial fibrin gel, our microfluidic system provides a valid and robust screening platform for the testing of newly developed *in situ* cross-linking polymers (e.g. elastin-based hydrogel), which are capable of mimicking specific features of the native cardiac ECM.

The simple insertion of a pair of electrodes in the culture medium reservoirs allowed to provide a controlled pacing to the constructs, thus assessing their electro-physiology. It is worth noting that the same configuration could be used to provide cells with an electro-mechanical stimulation to further favour cardiac maturation during culture.

In conclusion, this device enables the generation of cardiac micro-tissue, and its direct visualization and quantitative analysis, under controlled conditions, in ways that have not been possible in traditional cell culture or animal models. The ability to generate 3D cardiac constructs properly differentiated by means of controlled cyclic strain directly on-chip makes this microdevice an innovative and low-cost screening platform to enhance the predictive power of *in vitro* or *in silico* models.

Materials and Methods

Device design and fabrication

The device is composed by three layers of polydimethylsiloxane (PDMS, Sylgard 184, Dow Corning) polymerized in defined casts at 10:1 weight ratio of PDMS base to curing agent at 65 ºC for at least 3 hours Master molds were fabricated in a clean room environment using standard photolithography techniques with SU-8 2050 photoresist (MicroChem) and 4" silicon wafers as substrates. The cross-sectional size of the features was 1.6 mm (width) x 100 μm (height) for the top layer, and 1.6 mm (width) x 50 μm (height) for both middle and bottom layers (Fig. 1c). In addition, top and bottom layers included two rows of posts. Posts in the top layer were hexagonal in shape (side 28 μm), with a gap of 50 μm between posts in the same rows, and a distance of 300 μm between rows. Posts in the bottom layer were circular in shape (radius 30μm), with a space of 200 μm between posts in the same rows, and a distance of 500 μm between rows. The total thickness of the middle and bottom layers was maintained around 300 μm by dosing the amount of PDMS poured on their master molds, to ensure imaging compatibility with standard inverted fluorescence and confocal microscopes (Fig. 1f).

The PDMS stamps were peeled off the molds and assembled layer-by-layer as depicted in Fig. 1c. Briefly, surfaces containing features of top and middle layers were treated with air plasma (Harrick Plasma Inc) and brought in conformal contact after careful manual alignment to achieve irreversible bonding. After 30 minutes of incubation at 80 °C, the cell culture compartment was finalized by punching access ports through biopsy punchers: 500 μm holes for cell in/out ports and for the pressure line, and 5 mm holes for cell culture medium reservoirs (Fig. 1d). Upon a further air plasma treatment, the bottom layer was permanently bonded to the lower PDMS surface of the cell culture compartment after careful manual alignment, and allowed to cure overnight at 80 °C.

As shown in the top-view picture (Fig. 1e), the final device featured two compartments having similar layouts (1.6 mm wide and 10 mm long) and separated by a PDMS membrane with a thickness around 300 μm (Fig. 1f).

Finite element analysis (FEM)

Geometry of the model - Owing to the periodicity of the platform structure, only one periodic cell was considered and, owing to the symmetry of the periodic cell, only half of it was actually modelled, which consisted in PDMS membrane, PDMS pillar, and gel (Fig. S2a). The membrane and the pillar were discretized into 5'000 and 38'800 quadratic hexahedral elements (ABAQUS C3D20 elements), respectively. The gel was discretized into 64'000 linear hexagonal elements with hybrid formulation (C3D8H), which are more suitable when modeling nearly incompressible bodies involved in contact problems (Fig. S2b).

Modelling of material properties - The non-linear mechanical response of PDMS was modelled as non-linear elastic and isotropic, through a Mooney-Rivlin model:

$$W = C_1(\bar{I}_1 - 3) + C_2(\bar{I}_2 - 3)$$

where I_1 and I_2 represent the first two invariants of the deviatoric component of the right Cauchy-Green strain tensor, and material constants C_1 and C_2 were set to 254 and 146 kPa, respectively[31]. The fibrin hydrogel with fibrinogen concentration of 20 mg/ml was modeled as a linear elastic and isotropic material, with Young modulus equal to 10 kPa[32, 33], and Poisson ratio set to 0.4; this value was chosen despite the almost incompressible behavior of swollen hydrogels, so to account for the lower cohesion of a hydrogel as compared to a solid material.

Boundary conditions and contact interactions - Symmetry kinematic boundary conditions were imposed to account for periodicity and symmetry of the system, while the outer boundary of the PDMS membrane was prevented from any rigid motion (Fig. S2c). A uniform pressure linearly increasing up to 700 mmHg was applied on the lower surface of the PDMS membrane. Gel-pillar, gel- membrane and pillar-membrane contacts were modeled as frictionless, and a non-linear penalty method was used to describe the relationship between surface distance and contact pressure.

Device actuation

The system illustrated in Fig. S3 was assembled to perform the cyclic mechanical stimulation. A compressed air cylinder was used as a pressure source, while the pressure level was controlled and maintained constant through a precision regulator (IR1000, SMC). A three-way miniature valve (MH-1, Festo AG & Co. KG) was used to transmit to its output either the controlled pressure line or the atmospheric pressure. A ramp of stopcocks was connected to the miniature valve outlet to multiply the number of addressable microfluidic devices. Switching between input pressure values was achieved through a custom-made electronic controller based on the Arduino Uno microcontroller board (www.arduino.cc), whose square wave signal was properly amplified. The stimulation frequency could be regulated according to each experimental design.

Device mechanical characterization

To establish a target pressure that guaranties the contact between the PDMS membrane and the micro-posts, a preliminary characterization of microdevices (n=16) was performed to find the correlation between applied pressure and membrane displacement (see Fig. S4). To this purpose, the actuation chambers of a microfluidic device was filled with PBS, while a blue dye solution was injected into microfluidic chamber. The pressure was then gradually increased (from 0atm to 1.3atm, steps=0.1atm) and images were acquired by a camera connected with a stereomicroscope (Olympus SZ51). For each pressure increment, the white intensity of the micro-posts bottom surfaces was then quantified and used as an estimator for monitoring the membrane displacement. In details, in the initial condition (no pressure applied in the actuation chamber), the gap between micro-posts and membrane resulted completely filled by the blue dye solution. In this condition, the micro-posts bottom surfaces resulted blue coloured. By increasing the pressure level within the actuation chamber from 0atm to 0.4atm, the resulting gradual displacement of the membrane towards the micro-posts caused a reduction of this gap and a consequent whitening of the micro-posts bottom surfaces (“approach” phase in the Fig. S4). When the contact was reached, the gap was not filled anymore by the blue dye solution, and the micro-posts bottom surfaces appeared

white ("resist" phase in the Fig. S4). In this condition, corresponding to a pressure range between 0.5atm and 0.9atm, the normalized white intensity stabilized around an asymptotic value indicating the micro-post are resisting to the applied pressure. Further increases in the applied pressure caused the collapse of the micro-posts, which started to bend causing the white intensity value to diverge from the plateau ("collapse" phase in the Fig. S4). Fig. S4 shows the normalized white intensity of the micro-posts bottom surfaces plotted as a function of the pressure level applied in the actuation chamber. From the obtained curve, we estimated 0.5atm to be the minimum pressure value required to reach the contact and thus we set this pressure as the target stimulation for the following experiments.

Cyclic strain characterization

Experimental strain characterization was performed by tracking the displacement of spherical beads embedded in fibrin gel throughout the cycle of mechanical stimulation. In details, dark red polystyrene beads of 10 μm in diameter (Sigma-Aldrich) were suspended in PBS, vortexed for 1 min to break up bead aggregates, and mixed with fibrinogen (20 mg/ml) and thrombin (5 U/ml) solutions in order to reach a final concentration of 1.45×10^4 beads/μl. The obtained beads-laden fibrin pre-polymer solution was manually injected into the culture channel of microfluidic devices (0.45 μl/device). For each device a tygon tubing (0.5 mm ID, 1.5 mm OD) connected to a 1ml syringe, previously filled with ice-cold PBS, was loaded with the solution and plugged to the cell inlet port by means of a stainless steel coupler (0.5 mm ID, 0.7 mm OD). Subsequently, PBS solution was injected in the culture wells to completely fill the side channels. Mechanical characterization was thus performed stimulating 3D gel constructs at 1 Hz of frequency with a pressure square wave switching between 0 and 0.5 atm. Each microfluidic device was filmed throughout the experiment at a frame rate of 50 fps using a motorized inverted microscope (Olympus IX81); three constructs were considered in this analysis. Frames corresponding to deformed and non-deformed conditions were selected and analysed with ImageJ software. As

schematically indicated in Fig. 2d, nominal strains in the x-direction (ε_{xx}) were calculated from the measurements of the maximal displacement along the x-axis of couples of beads approximately aligned in the z-direction and located at opposite sides with respect to the longitudinal symmetry axis of the cell culture channel. Similarly, z-nominal strains (ε_{zz}) were calculated from the measurements of the maximal displacements along the z-axis of couples of beads approximately aligned along the x-axis. Mean and standard deviation (SD) of the measured ε_{xx} and ε_{zz} were calculated.

Nominal ε_{xx} and ε_{zz} values were also extracted from the numerical model, by replicating the procedure adopted when tracking the displacement of reference points on top view images on the computational grid to measure the nominal strains in the x- and z- direction at different locations within the gel. For each strain component, 15 nodes of the computational grid, located on 5 different levels equally spaced along the gel thickness (i.e. y-axis), were considered in the undeformed and deformed configurations.

For each level, three nodes were selected; when measuring ε_{xx} values, these were aligned along the z direction, approximately 30 μm from the gel boundary interacting with the pillar (Fig. S5, left hand column).

Owing to the symmetry of the system, ε_{xx} was measured as:

$$\varepsilon_{xx} = \frac{(x_F - x_{sim}) - (x_0 - x_{sim})}{(x_0 - x_{sim})} = \frac{x_F - x_0}{(x_0 - x_{sim})}$$

where x_0 and x_F are the x-coordinates in the undeformed and deformed configurations, while x_{sim} is the x-coordinate of the hydrogel yz-plane of symmetry.

When measuring ε_{zz}, the three selected points at each level were located approximately 100 μm from the gel boundary surface identified by the xy plane (Fig. S5, right hand column). Owing to the periodicity of the system along the z-direction, ε_{zz} was measured as:

$$\varepsilon_{zz} = \frac{(z_F - z_{sim}) - (z_0 - z_{sim})}{(z_0 - z_{sim})} = \frac{z_F - z_0}{(z_0 - z_{sim})}$$

Mean and standard deviation of the 18 measurements of ε_{xx} and ε_{zz} were calculated.

Mean and standard deviation (SD) of the measured ε_{xx} and ε_{zz} were compared to the corresponding experimental counterparts (Fig. 2d)

Cell isolation and characterization

Neonatal rat cardiomyocytes were isolated from 2-3 day-old Sprague Dawley rat hearts[34, 35] according to Swiss Federal guidelines for animal welfare and all procedures were approved by the Veterinary Office of the Canton Basel (Basel, Switzerland). Briefly, ventricles were digested first overnight in a 0.06% (w/v) solution of trypsin in Hank's balanced salt solution (HBSS, Gibco) and then in a 0.1% (w/v) solution of type II collagenase (Worthington Biochemical Corporation, Lakewood, NJ) in HBSS for a series of steps of 4 min at 37 °C and 150 rpm. Pre-plating in polystyrene culture flasks for a 75-min period was used to enrich the population for cardiomyocytes. In order to characterize the initial cell population, cells were seeded either in monolayer at a density of 60'000 cells/mm^2 or in 3D constructs for 4 hours. After immunofluorescence staining, relative fractions of neonatal rat cardiomyocytes (cardiac Troponin I -cTpn I- positive cells) and cardiac fibroblasts (vimentin positive cells) normalized to the total cell number (quantified by the number of nuclei, stained with DAPI) were assessed by image analysis.

Cell culture and stimulation

3D micro-cardiac constructs were generated by either overnight pre-cultured neonatal rat cardiac cells or freshly thaw human iPSC-derived cardiomyocytes (purchased by Cellular Dynamics International) suspended into a fibrin gel matrix into the microfluidic platform. In details, a fibrinogen solution (20 mg/ml in sodium chloride) was mixed to a cardiac cell suspension at a final concentration of 1×10^5 cells/µl and allowed to polymerize by adding thrombin (5 U/ml in calcium chloride). The cell-laden fibrin pre-polymer solution was manually injected into the culture channel of microfluidic devices (0.45 µl/device) and incubated for 10 minutes (5% CO_2 and 37 °C) before filling the lateral channels with culture medium (DMEM (Sigma Aldrich) supplemented with 1%

Hepes (Life Technologies), 1% penicillin-streptomycinfungizone (antibiotic-antimycotic, Life Technologies), 1% L-glutamine (Sigma Aldrich) and 10% fetal bovine serum (FBS, HyClone Inc, Logan, UT) and with 1.15 TIU/ml of aprotinin (Sigma Aldrich)). A cyclic mechanical stimulation (10% uniaxial strain, frequency 1 Hz) was thus applied for 5 days to 3D micro-cardiac constructs (Movies S3 and S4, representative of the low and high cell density, respectively). Statically cultured 3D constructs were used as control.

Cell viability

Cell viability was assessed in both stimulated and control 3D micro-cardiac tissues after 4 days in culture, by performing a LIVE/DEAD Assay (Life Technologies) according to the manufacturer's protocol. After washing with PBS, devices were perfused with a 2 μM calcein AM and 4 μM Ethidium homodimer-1 solution and subsequently incubated for 30 mins at 37°C. Confocal images of labelled cells were acquired with a fluorescence CLSM (Zeiss LSM 710 confocal microscope) equipped with Zen software. Green-labelled live cells and red-stained nuclei of dead cells were quantified using ImageJ software and normalized to the total cell number. Three samples for each condition were considered.

Immunofluorescence staining

Immunofluorescence analyses were performed on 3D micro-cardiac tissues directly within the microdevices right after injection or after 5 days of culture. Samples were fixed in 4% paraformaldehyde (PFA) for 45 minutes and incubated with 5% donkey serum, 2% bovine serum albumin (BSA) and 0.3% Triton (Sigma) PBS solution for 1 hour at 4°C to permeabilize cells and to block nonspecific bindings. Samples were incubated overnight at 4°C with the primary antibodies. Goat anti-rat vimentin (dilution 1:50, Santa Cruz Biotechnology) was used to distinguish fibroblasts. Mouse anti-rat cardiac Troponin I (cTpI, dilution 1:150, Abcam), rabbit anti-rat connexin43 (Cx43, dilution 1:150, Life Technologies), and mouse anti-rat sarcomeric α-

actinin (dilution 1:100, Abcam) were used to assess cardiomyocyte maturation and morphology. Cell proliferation was evaluated by staining for rabbit anti-rat Ki67 (dilution 1:100, Abcam). DAPI staining was used to identify the cell nuclei. Fluorescently labeled secondary antibodies (Life Technologies) were used at 1:200 for 6 hours at 4°C.

Image analysis

Relative fractions of proliferating cells were quantified normalizing the number of cells positive for Ki67 to the total cell number (quantified by DAPI). Cx43 expression was quantified by dividing the total Cx43-positive area normalized to the total number of cardiomyocytes, defined as cardiac troponin I-positive and vimentin-negative cells. Representative images of three different regions of each cardiac construct were acquired with a 20x objective on a fluorescence CLSM (Zeiss LSM 710 confocal microscope) and analysed by using ImageJ software. All immunostained images have been acquired and showed with the same convention in the device orientation: in details, the two parallel rows of micro-posts are always located at the top and at the bottom of the images, respectively. All data were presented as mean ± standard deviation.

SEM analysis

For scanning electron microscopy (SEM) analysis, samples were fixed in 4% PFA, dehydrated with increasing concentrations of ethanol (30, 50, 70, 90, 100%), critical point dried and sputtered-coated with gold-palladium right before being examined in a Nova NanoSEM 230 scanning electron microscope operated at 5 kV.

TEM analysis

For transmission electron microscopy (TEM), samples were fixed in 2.5% glutaraldehyde and then soaked in PBS containing 1% osmium tetroxide, dehydrated in ascending concentrations of acetone (30, 50, 70, 90, 100%) and embedded in Epon 812. After the polymerization of the resin at 65 °C

for 2 days, 60 nm thick sections of the samples were obtained. Sections were placed on copper grids, stained for 60 min with 6% uranyl acetate and 2 min with lead citrate. Afterwards, the sections were examined under Morgegni FEI transmission electron microscope operated at 80 kV.

Quantitative real-time reverse transcriptase polymerase chain reaction (RT-PCR)

Micro-cardiac tissues were digested in TRI-Reagent (Sigma), total RNA was isolated following an adaptation of a previously described method[36]. cDNA was reverse-transcribed from mRNA with the Omniscript Reverse Transcription kit (Qiagen) at 37 C° for 60 min. Quantitative real-time PCR (qRT-PCR) was performed with TaqMan® Assays master mix (Life Technologies) using a ABI 7300 Real-Time PCR system (Applied Biosystems, Carlsbad, CA). To investigate the maturation degree of the cardiac sarcomere we assessed the ratio between the mRNA expression levels of MYH7 (Myosin heavy Chain β) / MYH6 (Myosin Heavy Chain α) and MYL7 (Ventricular Regulatory Myosin Light) / MYL2 (Atrial Regulatory Myosin Light). Additionally the expression of TNNI3 (cardiac troponin I) and of GJA1 (Connexin-43, a key protein for the formation of functional gap junctions) was evaluated. The relative expression levels of each single gene were normalised using CDH2 gene (glyceraldehyde 3-phosphate dehydrogenase, GAPDH) and calculated using the 2 ΔCt method. Primers and probes have been purchased by Life Technologies.

Functional analysis

Both stimulated and control micro-tissue constructs were daily monitored for spontaneous beating by acquiring representative high resolution videos (with at least 16 frames per second) in three different regions (quadruplicate for each experimental group).

After 5 days in culture, constructs were stimulated through carbon rod electrodes and connected to a custom made electrical stimulator as previously shown[37]. This pacing signal consisted of a square pulse (duration 4 ms) with tunable frequency (1-10 Hz) and amplitude (0-23 V).

Microdevices were observed under a 20x objective on an inverted microscope (Olympus IX81), equipped with motorized stage and a culture chamber for live-cell imaging that enabled tight control of environmental pH and temperature.

The excitation threshold (ETH) was determined for each μECT, by keeping constant the signal frequency at 1Hz, as the minimum amplitude of the pacing signal required to induce sustained synchronous contractions of the micro-cardiac construct, i.e. a beating rate of 60 bpm. The maximum capture rate (MCR) was determined for each μECT, by keeping constant the signal amplitude at a value 1.5-fold the specific ETH, as the maximum frequency at which the signal could pace the construct. Both these parameters were assessed as described by Tandon N. *et al.*[37].

The contraction rate was characterized using a custom-made motion tracking software analyzing bright field microscope movies made available by Healy's group[38] at http://gladstone.ucsf.edu/46749d811. Briefly, images were partitioned into an array of macroblocks and the motion of each block for subsequent frames determined via an exhaustive search block matching algorithm, yielding for every frame a corresponding array of motion vectors. Thus, tracings of motion velocity, characterized by subsequent contraction and relaxation peaks, could be determined, allowing for the calculation of parameters such as the contraction rate[15].

The contraction amplitude was defined as the percentage reduction of the micro-cardiac tissue width throughout a beating cycle. Such figure was estimated by evaluating the relative positions of pairs of marker points, placed in proximity of the borders of the construct (i.e. close to each of the pillars rows) and in between two consecutive pillars. The measurements were performed on recorded videos through ImageJ software with the TrackMate plugin. At least 5 pairs of marker points were used for each region considered.

Beating synchronicity

Pixel intensity mean and standard deviation for each video frame was calculated and the standard deviation for three representative areas was displayed in a graph. The variation of the pixel intensity

in time of the different regions was used to track the movement of the μECTs and evaluate the local synchronized beating. Intensities were normalized based on maximum and minimum values recorded.

Drug concentration-response

Drug concentration-response experiments were performed on human μECTs after 6 days of mechanical stimulation. A modified Tyrode's solution containing 0.9 mM NaH_2PO_4, 25 mM glucose, 0.2 mM $CaCl_2$, 0.08 mM $MgSO_4$, 5 KCl, 109 mM NaCl (Sigma-Aldrich) was used. After 15 min, the drug's response on the micro-cardiac tissue was recorded using an inverted Olympus IX81 microscope, equipped with a culture chamber for live-cell imaging that enabled tight control of environmental pH and temperature. A stimulator was used to provide electric pacing at 1Hz, with amplitude based on each specific identified ETH (amplitude set to 1.5-fold the ETH). The isoprenaline concentration was increased stepwise (10^{-12}–10^{-6} M), and corresponding movies were acquired at least at16 frames per second.

Acknowledgments

This study was partially supported by Fondazione Cariplo, grant no. 2012-0891.

Authors contributions

M.R. and A.M. conceived the project; M.R. conceived the device; M.R., C.C. and M.L. designed the device; C.C., M.L. and P.O. fabricated the device; E.V., C.C., M.L and A.R. implemented the FEM model and performed simulations; C.C. and M.L. performed the mechanical characterization of the device; A.M., C.C., M.L. and P.O. performed and analyzed the biological experiments; A.M., P.O. and G.C. performed pacing analyses; E.G. performed the real time RT-PCR analysis; A.M., P.O., E.V. and M.R. wrote the manuscript; all the authors contributed to the final draft.

References:

1. S. N. Bhatia and D. E. Ingber, *Nat Biotech*, 2014, **32**, 760-772.
2. D. Huh, B. D. Matthews, A. Mammoto, M. Montoya-Zavala, H. Y. Hsin and D. E. Ingber, *Science*, 2010, **328**, 1662-1668.
3. H. J. Kim, D. Huh, G. Hamilton and D. E. Ingber, *Lab Chip*, 2012, **12**, 2165-2174.
4. Y. S. Zhang, J. Aleman, A. Arneri, S. Bersini, F. Piraino, S. R. Shin, M. R. Dokmeci and A. Khademhosseini, *Biomedical materials*, 2015, **10**, 034006.
5. A. Agarwal, J. A. Goss, A. Cho, M. L. McCain and K. K. Parker, *Lab on a Chip*, 2013, **13**, 3599-3608.
6. T. Boudou, W. R. Legant, A. Mu, M. A. Borochin, N. Thavandiran, M. Radisic, P. W. Zandstra, J. A. Epstein, K. B. Margulies and C. S. Chen, *Tissue engineering. Part A*, 2012, **18**, 910-919.
7. H. Chen, J. Cornwell, H. Zhang, T. Lim, R. Resurreccion, T. Port, G. Rosengarten and R. E. Nordon, *Lab Chip*, 2013, **13**, 2999-3007.
8. Y. Tanaka, K. Morishima, T. Shimizu, A. Kikuchi, M. Yamato, T. Okano and T. Kitamori, *Lab Chip*, 2006, **6**, 362-368.
9. N. H. L. van den Heuvel, T. A. B. van Veen, B. Lim and M. K. B. Jonsson, *Journal of Molecular and Cellular Cardiology*, 2014, **67**, 12-25.
10. A. Salameh, A. Wustmann, S. Karl, K. Blanke, D. Apel, D. Rojas-Gomez, H. Franke, F. W. Mohr, J. Janousek and S. Dhein, *Circulation research*, 2010, **106**, 1592-1602.
11. X. Trepat, L. Deng, S. S. An, D. Navajas, D. J. Tschumperlin, W. T. Gerthoffer, J. P. Butler and J. J. Fredberg, *Nature*, 2007, **447**, 592-595.
12. J. Zhuang, K. A. Yamada, J. E. Saffitz and A. G. Kléber, *Circulation research*, 2000, **87**, 316-322.
13. E. Cimetta, A. Godier-Furnémont and G. Vunjak-Novakovic, *Current Opinion in Biotechnology*, 2013, **24**, 926-932.
14. I. K. Zervantonakis, S. K. Hughes-Alford, J. L. Charest, J. S. Condeelis, F. B. Gertler and R. D. Kamm, *Proceedings of the National Academy of Sciences of the United States of America*, 2012, **109**, 13515-13520.
15. A. Mathur, P. Loskill, K. Shao, N. Huebsch, S. Hong, S. G. Marcus, N. Marks, M. Mandegar, B. R. Conklin and L. P. Lee, *Scientific reports*, 2015, **5**.
16. N. Thavandiran, N. Dubois, A. Mikryukov, S. Massé, B. Beca, C. A. Simmons, V. S. Deshpande, J. P. McGarry, C. S. Chen, K. Nanthakumar, G. M. Keller, M. Radisic and P. W. Zandstra, *Proceedings of the National Academy of Sciences*, 2013, **110**, E4698-E4707.
17. C. S. Simmons, B. C. Petzold and B. L. Pruitt, *Lab Chip*, 2012, **12**, 3235-3248.
18. H. Parsa, K. Ronaldson and G. Vunjak-Novakovic, *Advanced drug delivery reviews*, 2015.
19. W. H. Zimmermann, K. Schneiderbanger, P. Schubert, M. Didie, F. Munzel, J. F. Heubach, S. Kostin, W. L. Neuhuber and T. Eschenhagen, *Circ Res*, 2002, **90**, 223-230.
20. H. Kurazumi, M. Kubo, M. Ohshima, Y. Yamamoto, Y. Takemoto, R. Suzuki, S. Ikenaga, A. Mikamo, K. Udo, K. Hamano and T. S. Li, *PloS one*, 2011, **6**, e28890.
21. A. Pavesi, G. Adriani, M. Rasponi, I. K. Zervantonakis, G. B. Fiore and R. D. Kamm, *Sci Rep*, 2015, **5**, 11800.
22. G. S. Ugolini, M. Rasponi, A. Pavesi, R. Santoro, R. Kamm, G. B. Fiore, M. Pesce and M. Soncini, *Biotechnology and Bioengineering*, 2015, n/a-n/a.
23. Y. N. Xia and G. M. Whitesides, *Angew Chem Int Edit*, 1998, **37**, 550-575.
24. C. P. Huang, J. Lu, H. Seon, A. P. Lee, L. A. Flanagan, H. Y. Kim, A. J. Putnam and N. L. Jeon, *Lab Chip*, 2009, **9**, 1740-1748.
25. E. Ghafar-Zadeh, J. R. Waldeisen and L. P. Lee, *Lab Chip*, 2011, **11**, 3031-3048.

26. M. D. Nguyen, J. P. Tinney, F. Ye, A. A. Elnakib, F. Yuan, A. El-Baz, P. Sethu, B. B. Keller and G. A. Giridharan, *Analytical chemistry*, 2015, **87**, 2107-2113.
27. G. Wang, M. L. McCain, L. Yang, A. He, F. S. Pasqualini, A. Agarwal, H. Yuan, D. Jiang, D. Zhang, L. Zangi, J. Geva, A. E. Roberts, Q. Ma, J. Ding, J. Chen, D.-Z. Wang, K. Li, J. Wang, R. J. A. Wanders, W. Kulik, F. M. Vaz, M. A. Laflamme, C. E. Murry, K. R. Chien, R. I. Kelley, G. M. Church, K. K. Parker and W. T. Pu, *Nat Med*, 2014, **20**, 616-623.
28. S. Schaaf, A. Shibamiya, M. Mewe, A. Eder, A. Stohr, M. N. Hirt, T. Rau, W. H. Zimmermann, L. Conradi, T. Eschenhagen and A. Hansen, *PloS one*, 2011, **6**, e26397.
29. I. C. Turnbull, I. Karakikes, G. W. Serrao, P. Backeris, J. J. Lee, C. Xie, G. Senyei, R. E. Gordon, R. A. Li, F. G. Akar, R. J. Hajjar, J. S. Hulot and K. D. Costa, *FASEB journal : official publication of the Federation of American Societies for Experimental Biology*, 2014, **28**, 644-654.
30. M. K. B. Jonsson, Q.-D. Wang and B. Becker, *ASSAY and Drug Development Technologies*, 2011, **9**, 589-599.
31. S. Hosmane, A. Fournier, R. Wright, L. Rajbhandari, R. Siddique, I. H. Yang, K. T. Ramesh, A. Venkatesan and N. Thakor, *Lab on a Chip*, 2011, **11**, 3888-3895.
32. Y.-S. Yu and Y.-P. Zhao, *Journal of Colloid and Interface Science*, 2009, **332**, 467-476.
33. L. Miao, S. Jianren, S. Ying, B. Christopher and C. Quanfang, *Journal of Micromechanics and Microengineering*, 2009, **19**, 035028.
34. A. Marsano, R. Maidhof, L. Q. Wan, Y. Wang, J. Gao, N. Tandon and G. Vunjak-Novakovic, *Biotechnology progress*, 2010, **26**, 1382-1390.
35. M. Radisic, A. Marsano, R. Maidhof, Y. Wang and G. Vunjak-Novakovic, *Nature protocols*, 2008, **3**, 719-738.
36. P. Chomczynski and N. Sacchi, *Analytical Biochemistry*, 1987, **162**, 156-159.
37. N. Tandon, C. Cannizzaro, P.-H. G. Chao, R. Maidhof, A. Marsano, H. T. H. Au, M. Radisic and G. Vunjak-Novakovic, *Nat. Protocols*, 2009, **4**, 155-173.
38. N. Huebsch, P. Loskill, M. A. Mandegar, N. C. Marks, A. S. Sheehan, Z. Ma, A. Mathur, T. N. Nguyen, J. C. Yoo, L. M. Judge, C. I. Spencer, A. C. Chukka, C. R. Russell, P.-L. So, B. R. Conklin and K. E. Healy, *Tissue Engineering Part C: Methods*, 2014, **21**, 467-479.

Figure Legends

Fig. 1.

Design of the 3D heart-on-a-chip microdevice. (a) The microfabricated heart-like device uses two compartmentalized PDMS microchambers, featuring configurable geometries and separated by a PDMS membrane. The top compartment is subdivided, by means of two rows of hanging posts, into a central channel and two side channels. Cardiac cells, suspended in a matrix of fibrin gel, fill the central channel and generate a 3D cell construct, while culture medium is replenished through the side channels. (b) By pressurizing the bottom compartment, the PDMS membrane deforms, compressing the 3D cell construct and eventually abutting against the posts ends. Due to the presence of openings between posts, the compression transduces into a prominently uniaxial strain applied to the 3D cell construct. A cyclic pressure signal can thus mimic physiologic and pathologic systolic and diastolic phases. (c) During the fabrication process, three PDMS layers are aligned and irreversibly bonded. The two upper layers form the cell culture compartment, while the lower layer contains the actuation compartment. (d) A 3D sketch of both compartments is shown in their entirety, together with the external connections. (e) Picture of an actual 3D heart-on-chip device viewed from above. (f) Scanning electron microscopy micrograph of a cross-section of the device, showing the two compartments (scale bar, 500 μm).

Fig. 2.

Gel strains finite element computation and experimental measurements. (a) Repetitive unit of the microfluidic channel in its unloaded configuration. The key elements of the repetitive unit are depicted: PDMS membrane and PDMS pillars (light grey), channel ceiling (transparent), and gel (bronze). (b) Repetitive unit of the microfluidic channel in its fully loaded configuration. (c) Finite element computation of the spatial distribution of gel normal nominal strains in the pillar-to-pillar direction (NE_{xx}), in the vertical direction (NE_{yy}), and along the axis of the microfluidic channel

(NE_{zz}). (d) Left hand side: measurement of gel strains through image analysis. Strains in the x and z direction are measured based on the changes in position of the cyan and red dots, respectively. The gel portion considered in the finite element simulation is silhouetted in white. Right hand side: experimental measurements (mean ± standard deviation) are compared vs. the equivalent measurements performed on the finite element model.

Fig. 3.

Effect of uniaxial 3D cyclic mechanical strain on cell proliferation and viability. (a) Representative images of the initial cell population composition after 4 hours in 2D or in 3D fibrin gel. Cardiomyocytes are identified by cardiac Troponin I (cTp-I) (in green) and fibroblasts by vimentin (in red) staining. Nuclei are stained by DAPI (in blue). (b) Representative images of immunofluorescent staining of micro-cardiac constructs for ki67 (proliferating cells in red) and for DAPI (cell nuclei in blue) after 1 day in culture, with quantification of the percentage of proliferating cells, calculated as the ratio between the total number of Ki67+ cells and the total number of cell nuclei ($N=4$, $p<0.005$). (c) Representative images of micro-tissues stained for live (green) and dead (red) cells after 5 days in culture, with quantification of the percentage of live cells, calculated as number of living cells normalized to the total number of cells ($N=4$, $p<0.05$). Scale bars =100 μm. All images present the two parallel rows of micro-posts located at the top and at the bottom of the field of view, respectively.

Fig. 4.

Effect of uniaxial cyclic mechanical strain on micro-cardiac constructs maturation. The effect of cyclic strain was evaluated after 5 days in culture within the microfluidic device. (a) Representative images of immunofluorescence for specific cardiac markers as sarcomeric-α-actinin (red). Cardiac troponin I (green) and gap junctions as connexin 43 (red) of control (b) and stimulated (c) groups. (d) Quantification of the total $Cx43^{+}$ area normalized to the total number of cardiomyocytes (N=8,

p<0.05). (e) Ratios of mRNA level expressions of myosin heavy chain-7 (MHC-7) and 6 (MHC-6) and myosin light chain 2v and 2a. All ΔCt values are normalized to the relative GAPDH (N=4, p<0.05). All scale bars=100 μm. All images present the two parallel rows of micro-posts located at the top and at the bottom of the field of view, respectively.

Fig. 5.

Functionality of rat micro-cardiac tissues. (a) Micro cardiac-construct spontaneous beating monitored in four different random areas (rectangles) in both stimulated and control conditions. (b) The beating synchronicity was estimated by quantifying the variation of the averaged pixel intensity (N.I.) during a contraction period, resulting in the effective overlap of all the contraction peaks only in the stimulated condition. Electrical functionality of control and stimulated constructs was assessed after 5 days in culture by evaluation of the excitation threshold (c), maximum capture rate (d) and the contraction amplitude (e) (N=3, p<0.05). Representation of the contraction rate typical of the control and the stimulated micro-tissues during spontaneous beating (f).

Fig. 6.

Effect of uniaxial cyclic mechanical strain on human micro-cardiac constructs. The effect of cyclic strain was evaluated after 5 days in culture within the microfluidic device. Representative immunofluorescence images of stimulated tissues for specific cardiac markers as cardiac Troponin I (a, b green), gap (connexin 43 in fuchsia, c) and adherens (N-cadherin in red, b) junctions. Spontaneous beating was observed after 2.5 days in culture (c). Electrical functionality was evaluated in terms of percentage of contraction amplitude, excitation threshold (ETH) and maximum capture rate (MCR) (N=3). Contraction rate measured in micro-cardiac constructs in response to an increased isoprenaline concentration (10^{-12}–10^{-6} M) in presence (+ES) or absence (-ES) of an electric pacing signal.

Statistical analysis was performed on +ES (in blue) and on –ES (in red) (* $p<0.05$, *** $p<0.0001$) (d). All scale bars=100 μm. All images present the two parallel rows of micro-posts located at the top and at the bottom of the field of view, respectively.

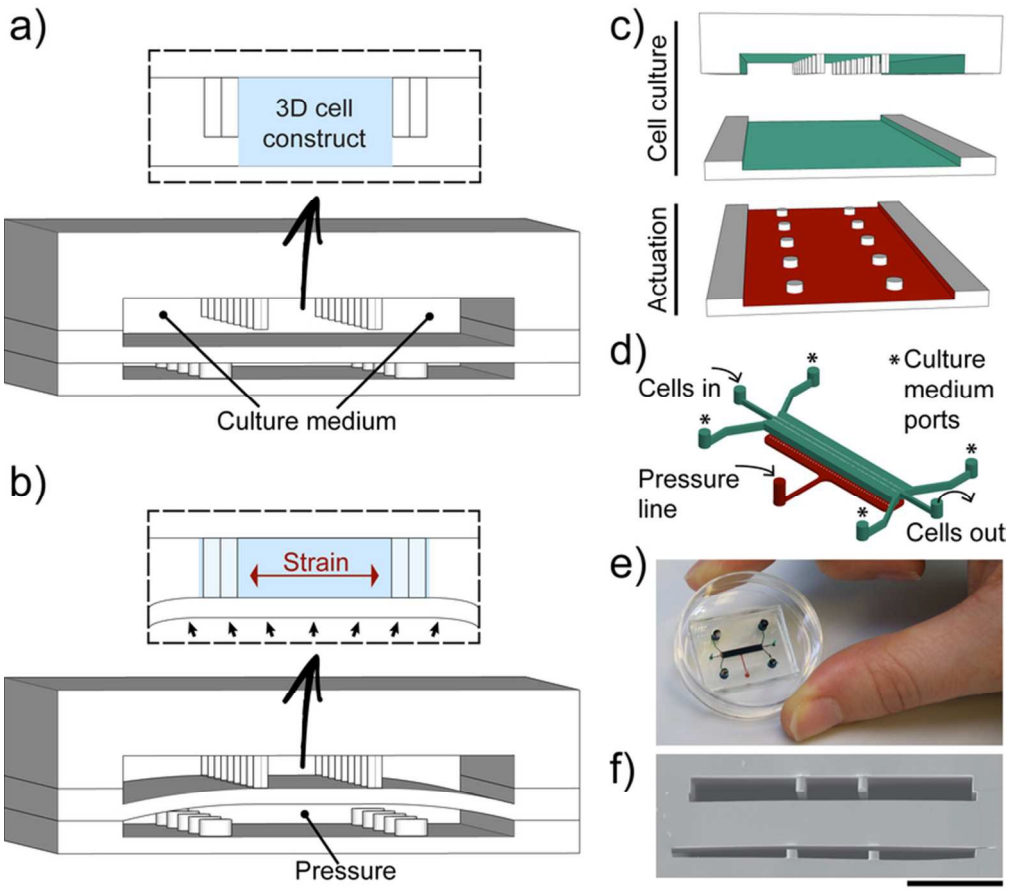

73x65mm (300 x 300 DPI)

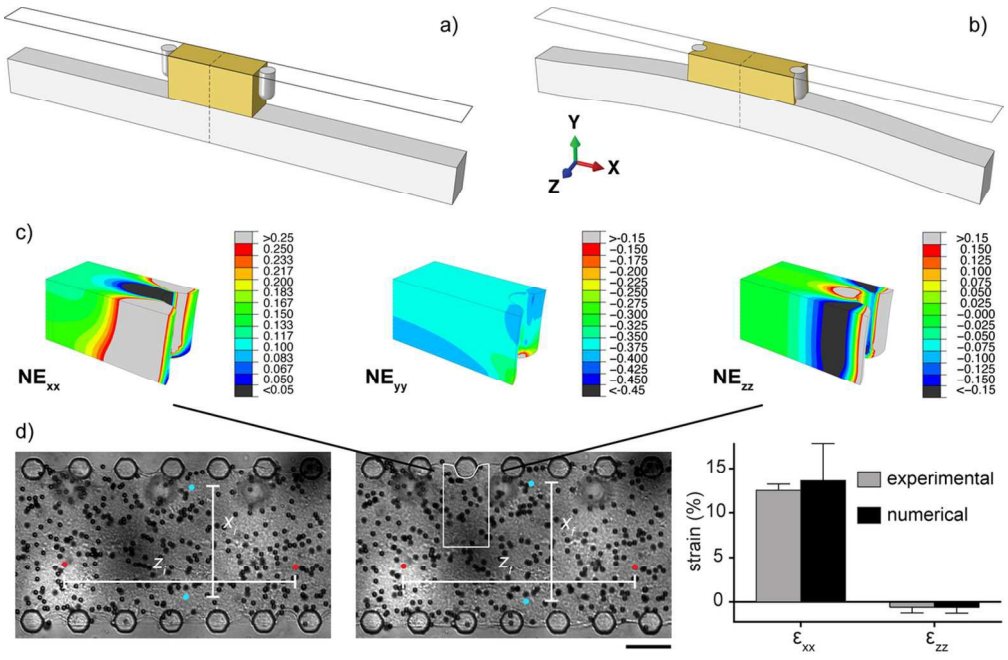

110x71mm (300 x 300 DPI)

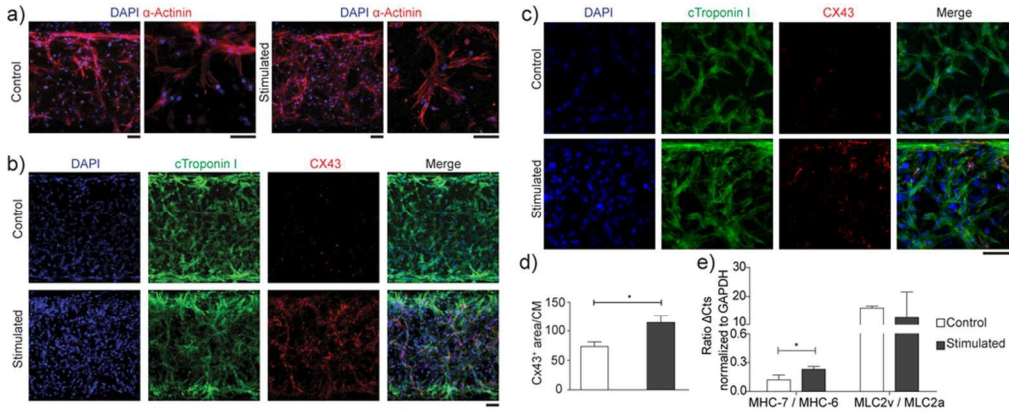

87x45mm (300 x 300 DPI)

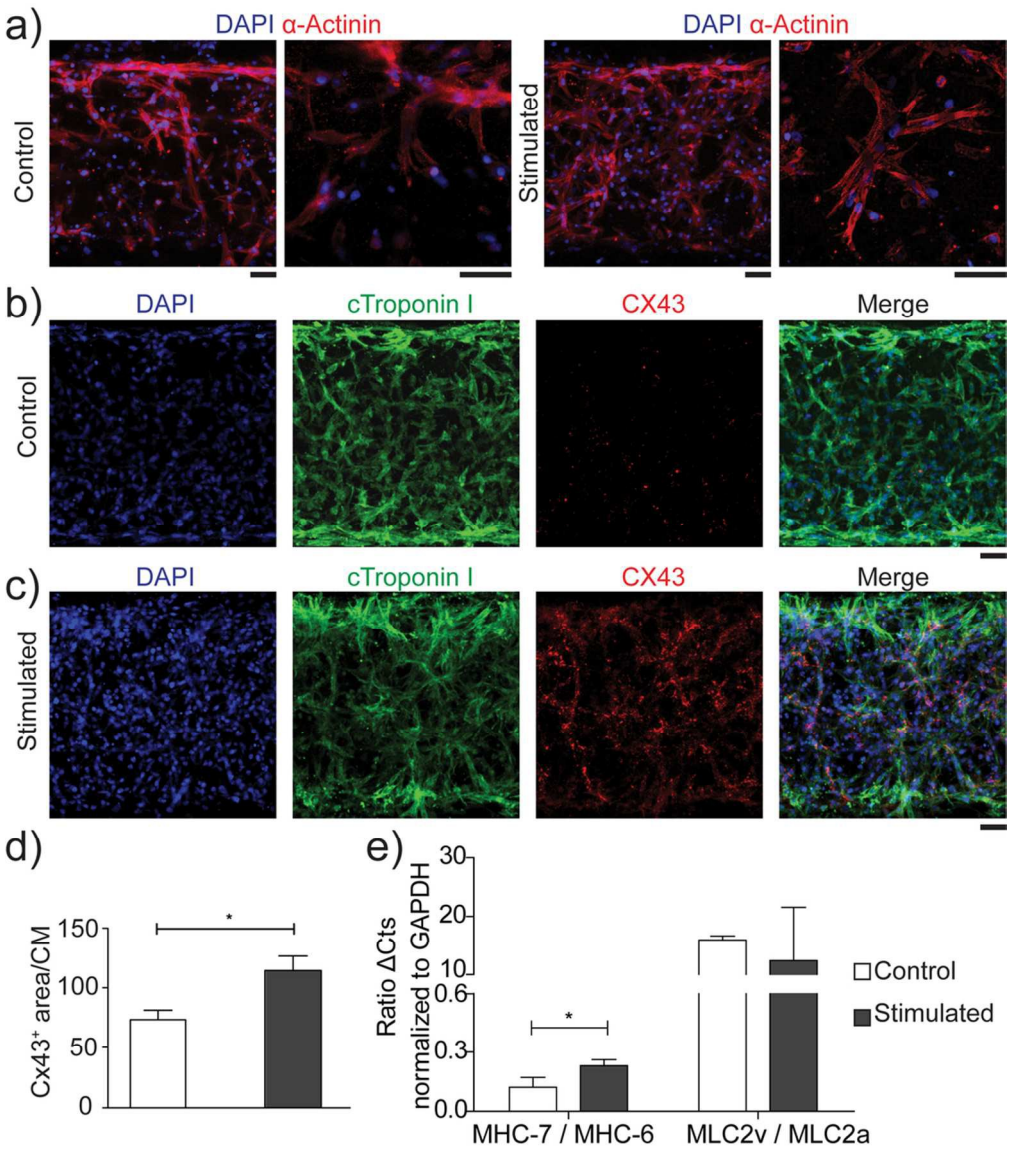

95x108mm (300 x 300 DPI)

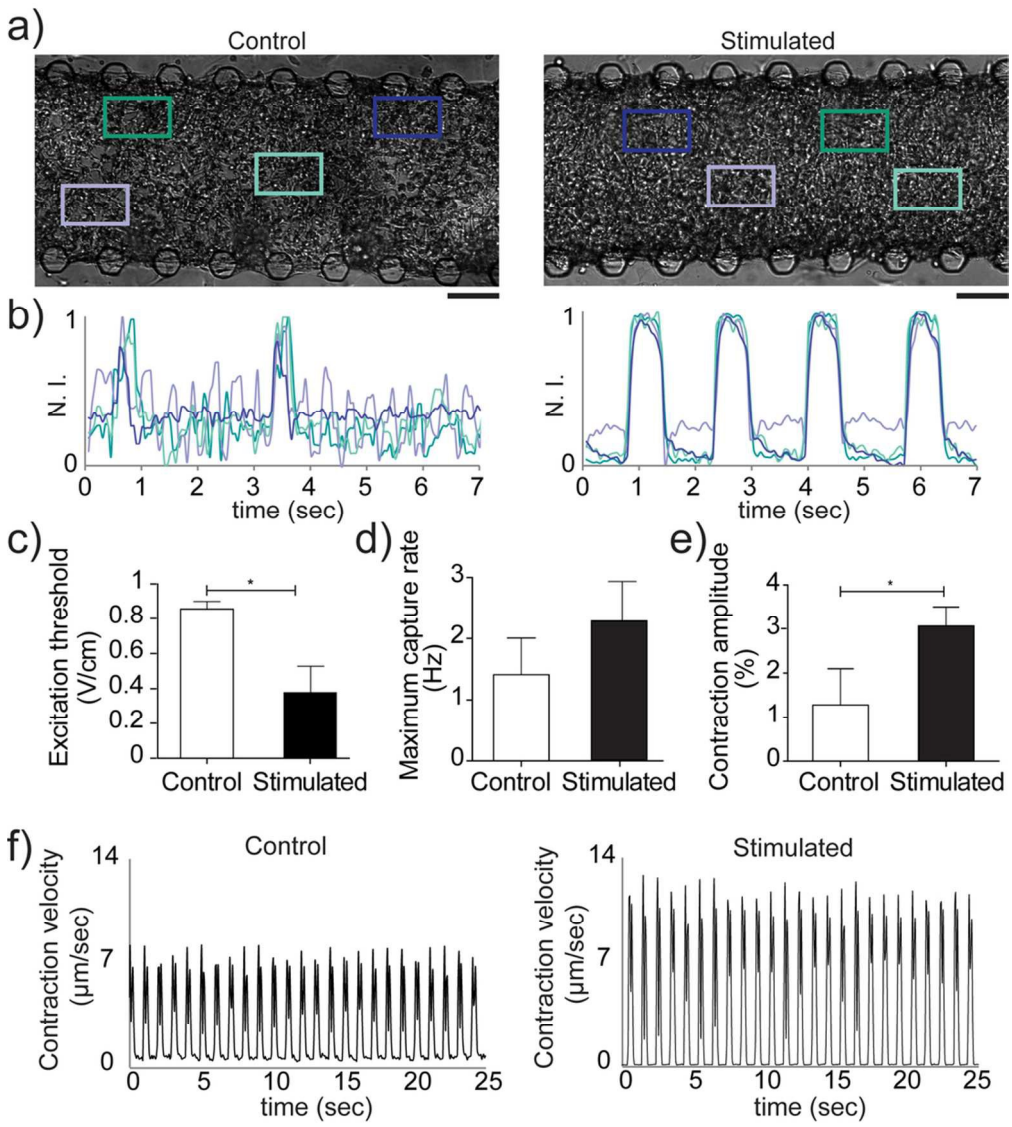

92x103mm (300 x 300 DPI)

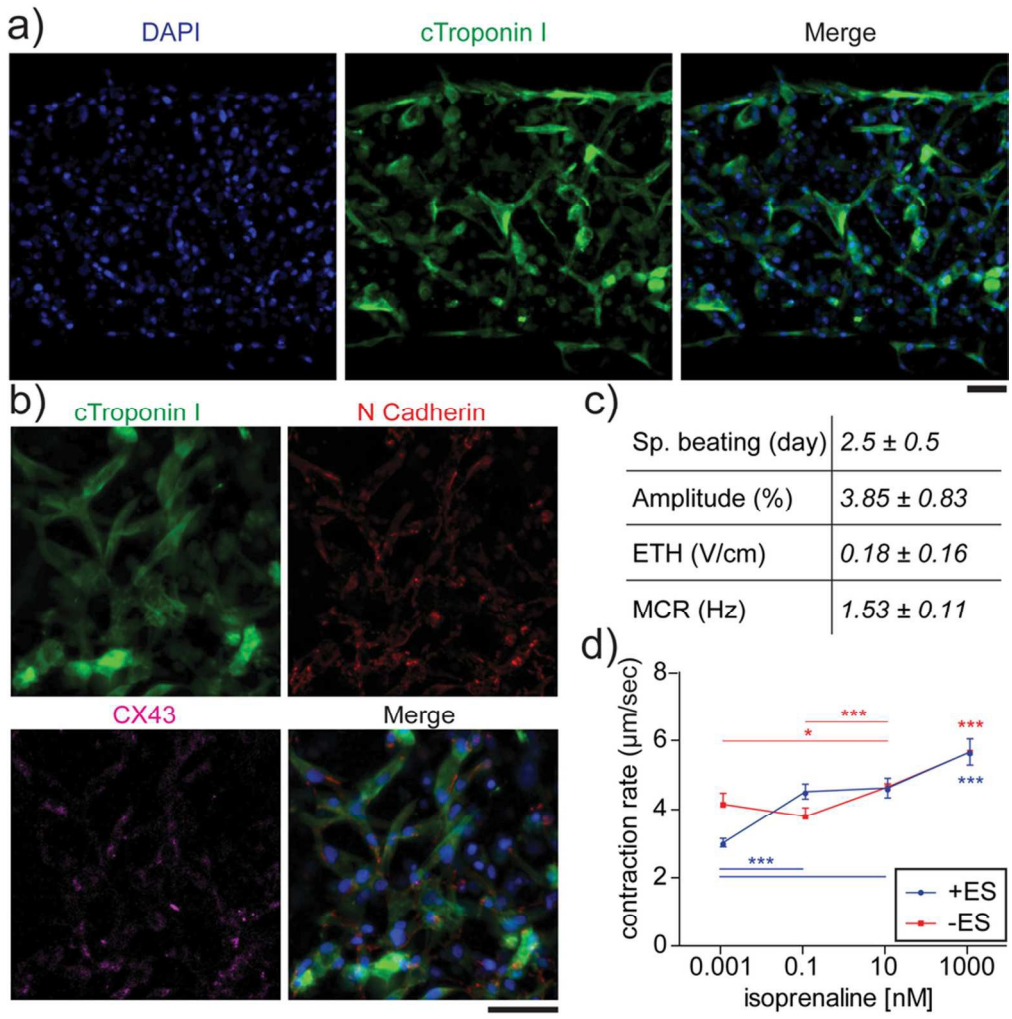

84x85mm (300 x 300 DPI)